



# Bioinspired porous microspheres for sustained hypoxic exosomes release and vascularized bone regeneration

Yike Gao<sup>a,1</sup>, Zuoying Yuan<sup>b,1</sup>, Xiaojing Yuan<sup>a</sup>, Zhuo Wan<sup>b</sup>, Yingjie Yu<sup>c</sup>, Qi Zhan<sup>d</sup>,  
Yuming Zhao<sup>a,\*\*</sup>, Jianmin Han<sup>e</sup>, Jianyong Huang<sup>b</sup>, Chunyang Xiong<sup>b,f,\*\*\*</sup>, Qing Cai<sup>c,\*</sup>

<sup>a</sup> Department of Pediatric Dentistry, Peking University School and Hospital of Stomatology, National Center of Stomatology, National Clinical Research Center for Oral Diseases, National Engineering Laboratory for Digital and Material Technology of Stomatology, Beijing, 100081, China

<sup>b</sup> Department of Mechanics and Engineering Science, College of Engineering, Peking University, Beijing, 100871, China

<sup>c</sup> State Key Laboratory of Organic-Inorganic Composites, Beijing Laboratory of Biomedical Materials, Beijing University of Chemical Technology, Beijing, 100029, China

<sup>d</sup> Tianjin Key Laboratory of Composite and Functional Materials, School of Materials Science and Engineering, Tianjin University, Tianjin, 300072, China

<sup>e</sup> Dental Medical Devices Testing Center, Dental Materials Laboratory, Peking University School and Hospital of Stomatology, Beijing, 100081, China

<sup>f</sup> Wenzhou Institute, University of Chinese Academy of Sciences, Oujian Laboratory, Wenzhou, Zhejiang, 325000, China

## ARTICLE INFO

### Keywords:

Hypoxic exosomes  
Stem cells from human exfoliated deciduous teeth  
Porous microsphere  
Sustained release  
Vascularized bone regeneration

## ABSTRACT

Exosomes derived from mesenchymal stem cells (MSCs) have demonstrated regenerative potential for cell-free bone tissue engineering, nevertheless, certain challenges, including the confined therapeutic potency of exosomes and ineffective delivery method, are still persisted. Here, we confirmed that hypoxic precondition could induce enhanced secretion of exosomes from stem cells from human exfoliated deciduous teeth (SHEDs) via comprehensive proteomics analysis, and the corresponding hypoxic exosomes (H-Exo) exhibited superior potential in promoting cellular angiogenesis and osteogenesis via the significant up-regulation in focal adhesion, VEGF signaling pathway, and thyroid hormone synthesis. Then, we developed a platform technology enabling the effective delivery of hypoxic exosomes with sustained release kinetics to irregular-shaped bone defects via injection. This platform is based on a simple adsorbing technique, where exosomes are adsorbed onto the surface of injectable porous poly(lactide-co-glycolide) (PLGA) microspheres with bioinspired polydopamine (PDA) coating (PMS-PDA microspheres). The PMS-PDA microspheres could effectively adsorb exosomes, show sustained release of H-Exo for 21 days with high bioactivity, and induce vascularized bone regeneration in 5-mm rat calvarial defect. These findings indicate that the hypoxic precondition and PMS-PDA porous microsphere-based exosome delivery are efficient in inducing tissue regeneration, hence facilitating the clinical translation of exosome-based therapy.

## 1. Introduction

Mesenchymal stem cells (MSCs) are a promising source for various cell-based regenerative therapies [1,2], and increasing researches have indicated that the therapeutic benefit of MSCs is primarily through paracrine effects [3,4]. Exosomes, small (30–150 nm in diameter) extracellular vesicles (sEVs) secreted by cells, play pivotal roles in paracrine effects by delivering mRNAs, miRNAs and proteins, etc. [5–7]. Compared with the traditional stem cell-based therapy, MSCs derived

exosomes show promising therapeutic potential as alternatives to living cells with equivalent or superior efficacy, but need no external maintenance [8–10]. For bone regeneration, although exosomes derived from varied MSCs can induce osteogenesis [11–13], the therapeutic efficacy is always confined due to the low retention and instability of exosomes. In addition, *in situ* bone regeneration is a well-organized process including but not limited to endogenous cell homing, angiogenesis and osteogenesis [14]. The MSCs derived exosomes suffer from limited potency, which makes it difficult to meet the abovementioned requirements [15].

Peer review under responsibility of KeAi Communications Co., Ltd.

\* Corresponding author. .

\*\* Corresponding author. .

\*\*\* Corresponding author. Department of Mechanics and Engineering Science, College of Engineering, Peking University, Beijing, 100871, China..

E-mail addresses: [yumingzhao70@sina.com](mailto:yumingzhao70@sina.com) (Y. Zhao), [cyxiong@pku.edu.cn](mailto:cyxiong@pku.edu.cn) (C. Xiong), [caiqing@mail.buct.edu.cn](mailto:caiqing@mail.buct.edu.cn) (Q. Cai).

<sup>1</sup> These two authors contribute equally.

<https://doi.org/10.1016/j.bioactmat.2022.01.041>

Received 1 December 2021; Received in revised form 16 January 2022; Accepted 24 January 2022

Available online 1 February 2022

2452-199X/© 2022 The Authors. Publishing services by Elsevier B.V. on behalf of KeAi Communications Co. Ltd. This is an open access article under the CC BY-NC-ND license (<http://creativecommons.org/licenses/by-nc-nd/4.0/>).

Hence, there is an urgent need to increase the potency of exosomes and effectively deliver these optimized exosomes to the bone defect site to induce vascularized bone regeneration.

*In vitro* cell culture is conventionally carried out under normal oxygen levels (21% O<sub>2</sub>) consistent with the atmospheric, which is much higher than the pO<sub>2</sub> in MSCs niche (e.g., 1–6% in the bone marrow). A large body studies have demonstrated that hypoxia culture of MSCs leads to enhanced secretion of various growth factors (GFs), as well as exosome cargo with improved therapeutic potential [16,17]. Recent works proved that the hypoxic condition of 1% O<sub>2</sub> induced the release of sEVs from various MSCs (e.g., bone marrow MSCs [18], and human umbilical cord MSCs [19]), hence enhancing the therapeutic efficacy of MSCs exosomes for treating multiple defects. However, the underlying mechanisms of how exosomes derived from varied MSCs sources after hypoxic pretreatment regulate biological responses, are still poorly understood.

The low retention and *in vivo* instability of exosomes is another major drawback preventing their positive therapeutic effects [20,21]. Similar to GFs or exogenous cell delivery, hydrogels have been served as exosome carriers, in the form of exosome encapsulation, to deliver exosomes into the target site and improve the local retention [22–24]. However, these exosomes cannot be long-term preserved in hydrogel, and the lyophilized exosome preservation method requires the addition of cryoprotectants (e.g., 1D-Trehalose) [25], which may cause adverse effects on metabolic or other biological processes for clinical application.

Surface adsorption *via* affinity coatings as another GFs delivery strategy [26,27], avoiding the lyophilization step, might be a more friendly way for transporting delicate exosomes. For such strategy, a bioinspired polydopamine (PDA) coating has been developed for rapid and stable exosome loading on poly(lactic-co-glycolic acid) (PLGA) scaffolds [28,29]. However, bulk scaffolds were mostly non-injectable, which may be inconvenienced in filling irregular-shaped defects. Microsphere-based biomaterials, as injectable micro-scaffolds with the advantage of minimally invasive manipulation for various tissue engineering applications [30–33], and we hypothesized that such kind of

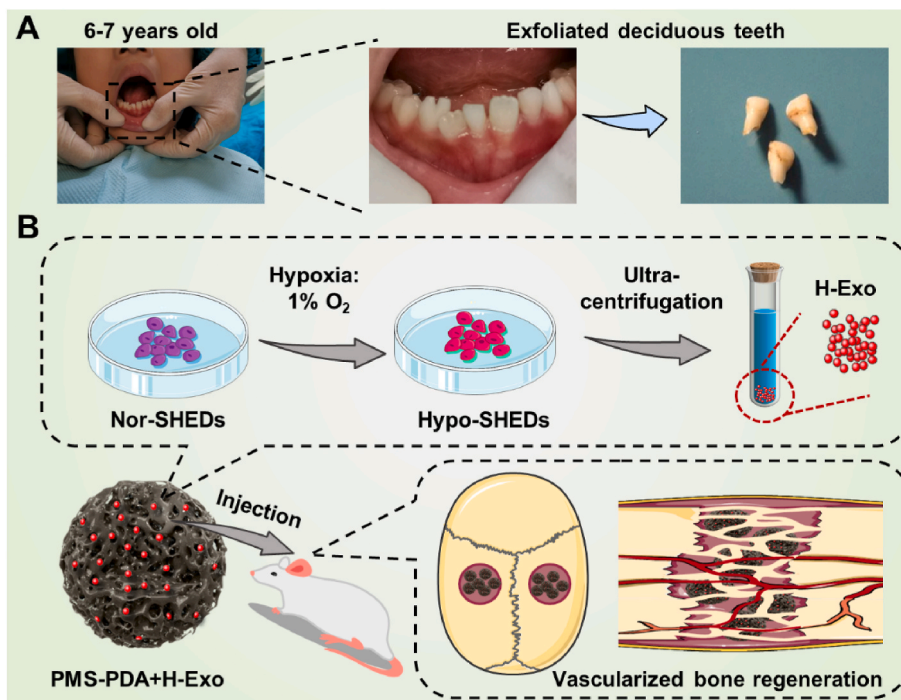
bioinspired modification on porous microspheres could effectively deliver exosomes, and fill irregular-shaped bone defects through minimally invasive surgery for further regeneration.

Stem cells from human exfoliated deciduous teeth (SHEDs), a unique kind of immature MSCs which is obtained noninvasively from the remaining pulp of detached deciduous teeth (Scheme 1A), have stronger proliferative capability and paracrine effects than widely used BMSCs [34–37]. In this study, we find that the hypoxic culture of SHEDs induced an increased release of exosomes by comprehensive proteomics analysis. Subsequently, SHEDs derived exosomes produced from different conditions (normoxia: Exo; hypoxic: H-Exo) were compared by high-throughput sequencing, proved that H-Exo exhibited enhanced cell recruitment and angiogenic potential, as well as superior osteogenesis through the upregulation of focal adhesion, VEGF signaling pathway, and thyroid hormone synthesis. To the best of our knowledge, this work does represent the first example of comprehensive proteomics of hypoxic SHEDs and high-throughput sequencing of hypoxic SHEDs derived exosomes. To effectively deliver these delicate exosomes *in vivo*, different from previous arts of bulk scaffolds, this work utilized bioinspired injectable porous PDA modified PLGA microspheres (PMS-PDA), resulting in the enhanced loading efficiency, optimized release profile and maintained bioactivity of exosomes from PMS-PDA. Finally, 5 mm rat calvarial defect model was established to identify the feasibility of using H-Exo functionalized PMS-PDA (PMS-PDA + H-Exo) in achieving vascularized bone regeneration (Scheme 1B). We expect that this systematic strategy can be generalized to control the release of various exosomes with optimized bioactivity for a broad range of clinical applications through minimally invasive surgery.

## 2. Results and discussion

### 2.1. Hypoxic pretreatment of SHEDs mediating the production and expression profiles of exosomes

SHEDs were identified by flow cytometry and were negative for CD45, while they were positive for the mesenchymal markers CD29 and



**Scheme 1.** A schematic illustration of the fabrication and application of PMS-PDA + H-Exo. (A) Images showing the source of human exfoliated deciduous teeth. (B) A schematic illustration showing the generation of exosomes from hypoxic pretreated SHEDs, and the rat model established to evaluate vascularized bone regeneration via injecting PMS-PDA + H-Exo into 5 mm rat calvarial defect. Photo credit: Y. Gao. PKUSS.

CD73 (Fig. S1). We firstly compared the comprehensive proteomics analysis of SHEDs incubated in common incubators (Nor-SHEDs) and SHEDs cultured in hypoxia environment (Hypo-SHEDs), which revealed the type and quantity of whole proteins after in cells. As shown in Fig. 1A, 164 proteins were up-regulated and 103 proteins were down-regulated in Hypo-SHEDs compared with the case of Nor-SHEDs. The differentially expressed proteins were analyzed with Gene Ontology (GO), which is a kind of bioinformatics analysis methods with three categories (Biological Process, Cellular Component and Molecular

Function) (Fig. S2). As expected, 6 proteins related to the function of “cellular response to hypoxia” (p value = 0.0020) were up-regulated (Fig. S3). In addition, the up-regulated proteins in the biological process category were enriched in “exocytosis” (p value = 0.0011) with changes in 18 proteins and “secretion by cell” (p value = 0.0014) with changes in 18 proteins, indicating the enhanced secretion behavior of SHEDs (Fig. S3). Note that the enriched proteins of Hypo-SHEDs in cellular components up-regulated “extracellular exosome” (p value = 0.0006) and “extracellular vesicle” (p value = 0.0006) functions,

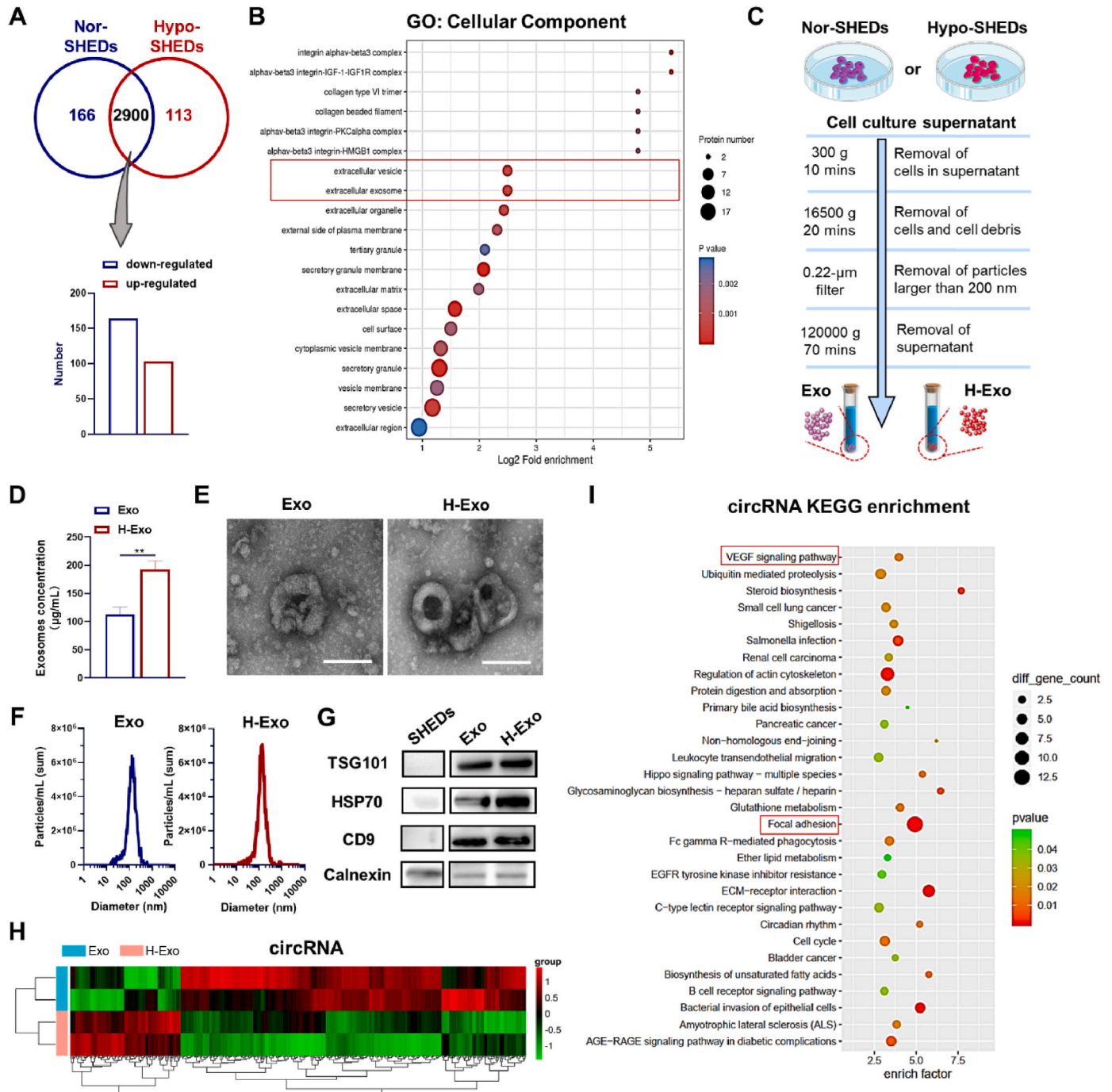


**Fig. 1.** Effects of hypoxic pretreatment on protein expression of SHEDs and the characterization of exosomal cargo. (A) Significantly upregulated and downregulated proteins (Hypo-SHEDs vs. Nor-SHEDs). (B) GO enrichment of up-regulated proteins in Hypo-SHEDs compared with Nor-SHEDs. (C) Technical illustration of the production of Exo and H-Exo. (D) Exosome protein concentration, (E) TEM images (scale bar: 100 nm), and (F) NTA analysis of Exo and H-Exo. (G) Western blot analysis of the expression of surface protein markers including TSG101, HSP70 and CD9. (H) Clustered heatmap of differentially expressed genes depicting the up and downregulated circRNAs and (I) corresponding KEGG enrichment of up-regulated circRNAs.

indicating changes in organelles, especially membrane-bound organelles (Fig. 1B).

The comprehensive proteomics analysis of Hypo-SHEDs indicated that the decreased oxygen level can influence the paracrine effects of SHEDs, by inducing exosome secretion with distinctive features, which can further communicate with vicinal or distant cells through internalization. Here, differential ultracentrifugation was utilized to purify exosomes derived from Nor-SHEDs and Hypo-SHEDs (Fig. 1C). The concentration of H-Exo was significantly higher than that of Exo after purification (\*\*p < 0.01) (Fig. 1D), a further proof that the hypoxia culture of SHEDs induced an increased release of exosomes, which is in consistent with the comprehensive proteomics analysis of SHEDs and previous report for HucMSC [19]. The morphology and the size of Exo and H-Exo were then characterized by transmission electron microscope (TEM) and nanoparticle tracking analysis (NTA). As shown in Fig. 1E and F, the Exo and H-Exo are both spherical with a similar size distribution (125.5 nm for Exo and 126.9 nm for H-Exo). Additionally, the surface protein marker expressions (TSG101, HSP70 and CD9) of Exo and H-Exo were confirmed by Western blots (Fig. 1G).

Variations in the gene expression conveyed by high-throughput RNA sequencing showed a statistically significant difference in H-Exo. The number of red spots represents the upregulated genes, while blue dots

represent the downregulated genes (Fig. S4A). Subsequently, hierarchical clustering was analyzed and the corresponding heatmap was depicted to display the upregulated circRNA, lncRNA or mRNA between two groups (Figs. 1H and S4B).

KEGG signaling pathway enrichment analysis was performed to reveal the possible pathways that H-Exo might regulate in relation to bone tissue regeneration. Of note, as shown in Fig. 1I, VEGF signaling pathway, which has been widely reported to play pivotal roles in the vascularization of regenerative tissue [38], was upregulated with an enrichment factor of 3.97 for circRNA pathway enrichment analysis. Additionally, 10 circRNAs related to focal adhesion were upregulated and could modulate cell behaviors in cell proliferation, migration, and further functional differentiation [39]. Thyroid hormone axis is essential in skeletal growth and maintenance, and effective bone defect regeneration [40,41]. The target genes related to thyroid hormone synthesis exhibited an upregulated expression both in mRNA (P < 0.05, enrich factor = 4.92) and lncRNA (P < 0.01, enrich factor = 3.63) pathway enrichment analyses (Figs. S4D and E). Taking the focal adhesion, VEGF signaling pathway and thyroid hormone synthesis together, H-Exo is expected to promote bone regeneration by homing endogenous cells, inducing angiogenesis and regulating bone metabolism.

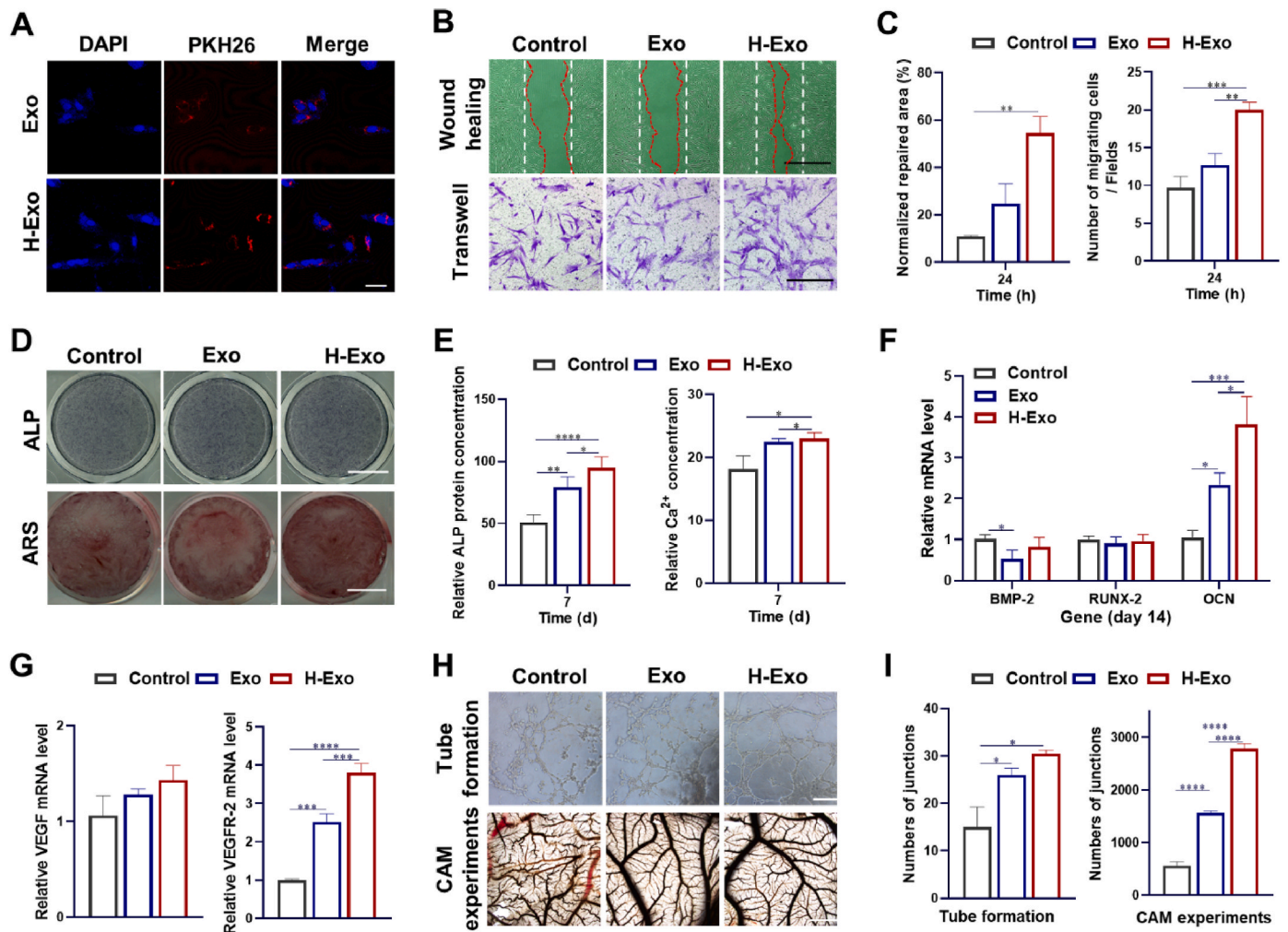


Fig. 2. H-Exo promote the proliferation, migration and osteogenic differentiation of BMSCs, and angiogenesis of HUVECs. (A) Cellular internalization of exosomes (PKH26) by BMSCs (scale bar: 20 μm). (B) Wound healing assay (scale bar: 1 mm) and Transwell assay on cell migration of BMSCs (scale bar: 450 μm), and (C) corresponding quantitative analysis. (D) ALP staining and Alizarin red staining (scale bar: 10 mm), (E) ALP protein activity and Ca<sup>2+</sup> concentration, and (F) the expression of osteogenic genes (BMP-2, RUNX-2, OCN) of BMSCs. (G) The expression of VEGF and VEGFR-2 genes in HUVECs cultured in medium supplemented with Exo or H-Exo. (H) *In vitro* tube formation of HUVECs (scale bar: 300 μm) and *In vivo* CAM assay for neovascularization (scale bar: 1 mm) with corresponding quantitative analysis of (I) numbers of junctions.

## 2.2. H-Exo promoting cell homing, osteogenesis and angiogenesis

SHEDs derived exosomes (Exo in this work), which have been reported to regulate angiogenesis and osteogenesis of BMSCs, were set as normoxia control [42]. Confocal images show that after 24 h incubation, a large number of PKH26-labeled exosomes (both Exo and H-Exo) were internalized by BMSCs (Fig. 2A). The proliferation of BMSCs grown in culture media supplement with Exo or H-Exo were determined by CCK-8 assay. As shown in Fig. S5, similar to the previous work, Exo group showed enhanced cell proliferation compared with TCPs, while the highest OD values were obtained in H-Exo groups.

In situ bone regeneration requires the homing of endogenous cells, which can further promote tissue remodeling [43–45]. Here, wound healing and Transwell assays (Fig. 3B and C) were employed to evaluate the migration of BMSCs. The normalized repaired area was  $55 \pm 7\%$  and the number of migrating cells per field was  $20 \pm 1$  in the H-Exo group, which was 2.2 times and 1.6 times higher than that in the Exo group, respectively. Generally, H-Exo showed significant promotion in the cell migration in both the horizontal and vertical directions (\*\* $p < 0.01$ ), followed by Exo, indicating potential endogenous stem cell homing to the injury site.

After incubation with Exo and H-Exo in osteogenic medium (OM) for 7 days, both ALP staining (Fig. 3D) and quantitative ALP activity determined by ELISA (Fig. 3E) were significantly enhanced, indicating higher ALP production by BMSCs. The Alizarin red staining and  $\text{Ca}^{2+}$  content at 14 days were also up-regulated in an increasing order of Control < Exo < H-Exo. We then selected three gene markers (BMP-2, RUNX-2, OCN) which are closely related to the osteogenic differentiation of BMSCs to evaluate the osteoinduction of Exo and H-Exo. Interestingly, the early marker of osteogenesis (BMP-2 and RUNX-2) demonstrated the highest expression in Exo (Fig. S6), while the highest expression of downstream OCN genes was found in H-Exo, which was 1.6 times higher than Exo group and 3.6 times higher than Control group (Fig. 3F).

Rapid and sufficient vascularization, which could transport nutrients and oxygen supply, and hence influence cell survival, plays a pivotal role in successful bone regeneration. Here, the internalization of exosomes, migration, angiogenesis maker expression and tube formation of HUVECs, as well as chick embryo chorioallantoic membrane (CAM) assay, were performed. After 24 h of incubation, obvious PKH26-labeled exosomes were also internalized by HUVECs (Fig. S7). Using wound healing (Figs. S8A and S8B) and Transwell assays (Figs. S8C and S8D), we found that H-Exo contributed to the migration of HUVECs with significantly higher normalized repaired area and number of migrating cells compared with Exo and Control. The VEGF and VEGF-R2 gene expression of HUVECs were up-regulated in H-Exo, and followed by Exo groups as shown in Fig. 2G. The *in vitro* (tube formation) and *in vivo* (CAM assay) model of neovascularization were subsequently carried out (Fig. 2H). H-Exo promoted tube formation with higher numbers of junctions (Fig. 2I) and total length (Fig. S9) compared to Control, followed by Exo. Similarly, CAM experiments demonstrated that both Exo and H-Exo treated groups formed higher numbers of vessels, while H-Exo treatment exhibited the highest numbers of junctions and total length. Taken together, H-Exo which secreted from hypoxia pretreated SHEDs demonstrated strengthened angiogenic potential.

## 2.3. Characterizations of PMS-PDA and PMS-PDA + H-Exo

Similar to protein GFs, surface coatings of biomaterials have been proven to deliver EVs both *in vitro* and *in vivo* [28,46,47]. PDA coating with satisfying adhesive property was shown to increase the loading of EVs onto biomaterials including PLGA scaffolds [29] and titanium oxide nanotubes [48], which could significantly prolong the release of EVs, nevertheless, the EVs loading efficiency in these reports was not characterized. Here, attributable to the bioinspired dopamine chemistry, injectable PMS-PDA porous microspheres were applied to adsorb

exosomes (Fig. 3A). As shown in Fig. 3B, porous PLGA microspheres (PMS) were fabricated with a size of  $235.7 \pm 30.5 \mu\text{m}$  in white, while a dark brown color was observed for PMS-PDA microspheres after PDA coating, and the average diameter was  $249.4 \pm 23.1 \mu\text{m}$ . PMS-PDA microspheres could adsorb PKH26-labeled exosomes (red dots in Fig. 3B) by soaking at  $4^\circ\text{C}$ . The elemental mapping of nitrogen signals (in green) in PMS-PDA indicated successful PDA coating (Fig. 3C). The exosomes functionalized microspheres were named as PMS-PDA + Exo or PMS-PDA + H-Exo, according to the applied exosomes. As an example, Fig. 3D shows the CLSM images that BMSCs (blue dots for DAPI) were cultured on PMS-PDA + H-Exo (red dots for PKH26-labeled H-Exo).

We continued to systematically study the loading efficiency and release profile of exosomes from PMS and PMS-PDA. The porous structure and PDA (polydopamine) modified surface make PMS-PDA microspheres reach the maximum loading rate of  $14.6 \pm 2.6 \mu\text{g}/\text{mg}$  microsphere after soaking for 4 h, while the PMS reached its maximum loading rate of  $2.5 \pm 0.5 \mu\text{g}/\text{mg}$  microspheres only after soaking for 6 h. (Fig. 3E). The *in vitro* release of exosomes was carried out at  $37^\circ\text{C}$ , 60 rpm over a period of 21 days. As shown in Fig. 3F, there was an obvious burst release of exosomes from PMS during the initial 3 days, and the release amounts were quite few in the following days. However, PMS-PDA exhibited sustained release (9.6% in 3 d, 48.3% in 7 d, 82.4% in 14 d and 90.2% in 21 d) of higher amounts of exosomes (1.4  $\mu\text{g}/\text{mg}$  PMS-PDA in 3 d, 7.1  $\mu\text{g}/\text{mg}$  PMS-PDA in 7 d, 12.0  $\mu\text{g}/\text{mg}$  PMS-PDA in 14 d and 13.2  $\mu\text{g}/\text{mg}$  PMS-PDA in 21 d) for a longer period (Fig. 3G). The structure of released exosome is still spherical without significant deformation.

We compared the loading efficiency and release kinetics of various surface coating methods including PDA, polyethyleneimine (PEI), tannic acid (TA) and heparin coating in Table S1. Although the scaffold materials were different, most studies showed that more than a half of loaded exosomes would be released within 1 d without affinity coatings, and almost no released exosomes could be detected after 7 d. Among the affinity coatings, few exosomes could be released from PEI coated scaffolds within 14 d due to the strong electrostatic interactions between PEI and exosomes [49]. In contrast, PDA or TA coatings achieved sustained release of exosomes (PDA coating: 20% in 1 d, ~80% in 8 d; TA coating: 50% in 3 d, ~90% in 14 d) for more than one week, which was attributed to the adhesive feature of catechol groups [28,46]. In particular, thanks to the porous micro-spherical structure, PMS-PDA showed superior control of exosome release kinetics (9.6% in 3 d, 48.3% in 7 d) compared with aforementioned catechol-functionalized bulk scaffolds.

The proliferation of BMSCs cultured on various microspheres was determined by CCK-8 assay as shown in Fig. 3H. Continuous cell proliferation was detected from day 1 to day 5, and the OD values of PMS and PMS-PDA had no significant difference with Control at day 5, indicating acceptable cytocompatibility of PLGA and PDA coating [50, 51]. Although there was no significant difference in the OD values of PMS-PDA + Exo and PMS-PDA + H-Exo, the introduction of Exo and H-Exo could enhance the cell proliferation on PMS-PDA significantly. After 5 days of culture, live/dead staining confirmed abundant live cells (green) attached on various microspheres, and few dead cell (red) could be detected (Fig. 3I). In the cases of PMS-PDA + Exo and PMS-PDA + H-Exo, the formation of microsphere-cell aggregates was observed, which may be due to the rich extracellular matrix secreted by attached BMSCs [52,53].

To determine whether the exosomes released from PMS-PDA + Exo and PMS-PDA + H-Exo were normal in biological functions, BMSCs were cultured on the lower chambers of Transwell plates in the presence of various microspheres in the upper chambers. ALP and Alizarin red staining, as well as ALP protein activity and  $\text{Ca}^{2+}$  concentration, were enhanced in PMS-PDA + Exo and PMS-PDA + H-Exo groups after induction by OM for 7 days (Fig. S10), which was in accordance with aforementioned results of free exosomes supplementation (Fig. 2B and

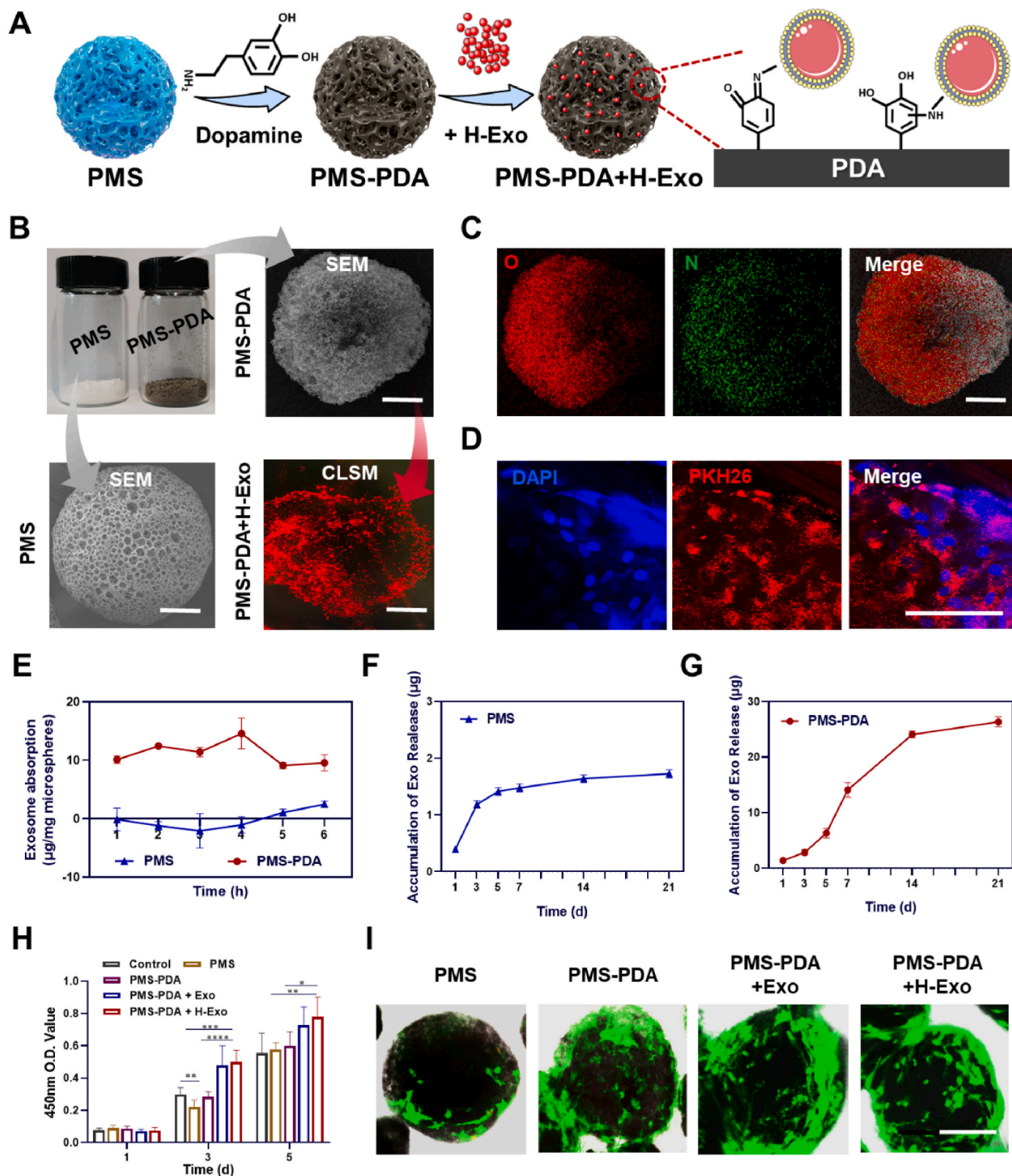


**Fig. 3.** Fabrication and characterizations of PMS-PDA and PMS-PDA + H-Exo. (A) Schematic illustration showing the PDA coating of porous PLGA microspheres and the subsequent exosome adsorption via bioinspired dopamine chemistry. (B) Optical image and SEM images of PMS and PMS-PDA, as well as the distribution of PKH26 labeled exosomes on PMS-PDA. (C) Elemental mapping images of PMS-PDA. (D) CLSM images of BMSCs cultured on PMS-PDA + H-Exo. (E) The loading efficiency curves over time for PMS and PMS-PDA. (F) The release profile of H-Exo from (F) PMS and (G) PMS-PDA. (H) Cell proliferation study of BMSCs cultured on various microspheres using CCK-8. (I) Live-dead assay staining of BMSCs cultured on various microspheres. (A-C, scale bar: 60 µm; I, scale bar: 100 µm).

C). In addition, the CAM experiments confirmed that the sustained release of exosomes could promote neovascularization *in vivo*, and PMS-PDA + H-Exo had improved angiogenic potential (Fig. S11).

#### 2.4. *In vivo* delivery of H-Exo by PMS-PDA promoting calvarial bone regeneration

Having confirmed the excellent biocompatibility and ability to control the exosome release kinetics of PMS-PDA, we continued to explore their *in vivo* regenerative efficacy. According to our previous works [54], 5 mm rat calvarial bone defects were established. Using PMS-PDA as an exosome-free control, PMS-PDA + Exo and PMS-PDA + H-Exo were injected into the 5 mm rat calvarial bone defects (Fig. S12). As shown in the micro-CT images (Fig. 4A), almost no new bone formation can be observed in Blank groups, and only a few bones newly formed at the edge of defects in the PMS-PDA group up to 8 weeks. The corresponding BV/TV (Fig. 4B) and BMD (Fig. 4C) values were  $18.4 \pm 6.8\%$  and  $213.0 \pm 41.0 \text{ mg/cm}^3$  for PMS-PDA, respectively, which were slightly higher than Blank groups. Exo had been proved to induce new bone formation to a certain extent, fragmentary bone tissues formed from the edge to the center of the defects were detected with much higher BV/TV ( $30.1 \pm 7.7\%$ ) and BMD ( $344.6 \pm 71.1 \text{ mg cm}^{-3}$ ) values at 8 weeks post-operation. More promisingly, the defect hole in PMS-PDA + H-Exo group was filled with abundant newly formed bone tissues at 8 weeks post-implantation contributed to the sustained release of H-Exo, and the BV/TV ( $58.8 \pm 5.9\%$ ) and BMD ( $529.5 \pm 59.3 \text{ mg cm}^{-3}$ ) values were significantly higher than other groups.

The sections of calvarial bone were stained with hematoxylin-eosin (H&E) and Masson's trichrome for histological analysis (Fig. 4D). From 4 weeks to 8 weeks post-operation, the defect areas in the Blank groups filled with a thin layer of fibrous tissues, while collagen deposition can be observed in PMS-PDA groups which may contribute to the porous architecture of PMS-PDA. Both the PMS-PDA + Exo and PMS-PDA + H-Exo groups exhibited collagen-rich extracellular matrix with remarkable new bone formation in the defect areas. Delightedly, we observed abundant highly vascularized bone tissue in PMS-PDA + H-Exo groups 8 weeks post-operation, which is consistent with the micro-CT results. In addition, the degradation of microspheres was observed from 4 to 8 weeks, providing spaces for new bone formation alongside their degradation (Fig. S13).

Immunohistochemical staining of OCN, which is highly expressed in mature bone tissue, was conducted (Fig. 5A). At 8 weeks post-operation, OCN was intensively expressed in the newly formed bone tissue, and the highest expression of OCN was found in the PMS-PDA + H-Exo group, further proving that the sustained release of H-Exo from the PMS-PDA microspheres accelerated the new bone formation.

To reveal the process of new bone formation induced by PMS-PDA + H-Exo, immunohistochemical staining of PCNA, CD31 and COL-1 was evaluated (Fig. 5B). The PCNA positive staining indicates actively proliferating host cells. At 4 weeks post-operation, there was a significantly higher PCNA expression in the PMS-PDA + Exo and PMS-PDA + H-Exo group compared with the PMS-PDA group. As the bone regeneration progressed, however, the brown color to show the PCNA activity turned weaker in PMS-PDA + H-Exo group at 8 weeks post-operation. Effective bone regeneration highly relies on sufficient vascularization, which plays a pivotal role in cell recruitment, nutrient and oxygen supply, and metabolism of waste [27,55]. Although angiogenesis occurs almost throughout the bone defect healing process, inducing angiogenesis at the early stage appears to be optimal [14]. Here, the levels of CD31 expression were displayed in the order of PMS-PDA + H-Exo > PMS-PDA + Exo > PMS-PDA groups at 4 weeks post-operation, and few positive staining can be observed in PMS-PDA + H-Exo group at 8 weeks post-operation, which was similar to the PCNA expression. In all three microsphere-filled groups, the COL-1 staining became thicker along with longer post-operation time, and the highest expression of COL-1 was identified in the PMS-PDA + H-Exo group. Furthermore, the systemic

toxicity of PMS-PDA + H-Exo was evaluated *in vivo* (Fig. S13). H&E staining images of main organs (heart, liver, spleen, kidney and brain) showed that the application of PMS-PDA + H-Exo did not cause any damage to the main organs.

As previous works report, although exosomes derived from various cell lines exhibited remarkable osteogenesis potential [13,28,29,56], the *in vivo* new bone formation (BV and BMD values) of defects treated with exosomes was always confined as shown in Table S2, and the probable reason may be the low retention and stability of exosomes *in vivo*, insufficient blood vessels and delayed ossification. Traditional therapeutic targeting of the vascularized bone regeneration is focus on growth factors (represented by vascular endothelial growth factor) delivery, however, the instability, immunogenicity, tumorigenesis, and high cost of GFs hinder their translational translation. Here, H-Exo with the significant up-regulation of focal adhesion, VEGF signaling pathway and thyroid hormone synthesis, could be sustainably released from PMS-PDA for more than 21 d. Endogenous cell homing, neo-vascularization, and bone metabolism were then accelerated, resulting in rapid vascularized bone regeneration (Fig. 5C). Attributed to the comprehensive proteomics analysis and high-throughput sequence, the findings of hypoxia-stimulated SHEDs derived exosomes and their roles in angiogenesis and osteogenesis may be in favor of the development of powerful therapeutic exosomes via hypoxic pretreatment, and the PDA coating modified porous PLGA microspheres could be ideal exosome carrier for various tissue engineering applications.

Compared with the current state of the arts, where exosomes were encapsulated in hydrogels, our strategy is based on a simple adsorbing technique. This technology is nonspecificity, enables the separate preservation of exosomes and exosome carriers, which could simplify the production and transportation processes. In addition, compared with bulk scaffolds, microsphere-based biomaterials have the advantage of minimally invasive manipulation, and such PMS-PDA microspheres are fabricated utilizing PLGA as matrix materials, which have been approved by the FDA with excellent biocompatibility. However, the materials were prepared in the form of microspheres for implantation in the present study, which is not suitable for a load-bearing bone defect including long bone defect. Incorporating these bioactive microspheres into hydrogels, bone cements, and 3D printing scaffolds may be one potential solution to expand this strategy to be useful in long bone defect. Overall, combining the simplicity, sustained release capability, safety, efficacy, convenient operation and general applicability of this approach, this exosome delivery platform to sustain the release of exosomes with optimized therapeutic potency can be translated toward a new class of exosome-based therapies.

### 3. Conclusion

In our study, the comprehensive proteomics analysis of hypoxia SHEDs and the high-throughput sequence of hypoxia SHEDs derived exosomes confirmed that hypoxic precondition induction could enhance secretion of exosomes from SHEDs, as well as regulate the transcriptomics of exosomes. H-Exo exhibited enhanced angiogenesis and osteogenesis capacity via the significant up-regulation of focal adhesion, VEGF signaling pathway and thyroid hormone synthesis. In view of the low retention and stability of exosomes *in vivo*, the fabricated porous PMS-PDA microspheres with an adsorption efficiency of  $14.6 \pm 2.6 \mu\text{g}/\text{mg}$  microspheres were able to prolong the release of H-Exo with high bioactivity. The promotion of PMS-PDA + H-Exo on stepwise vascularized bone regeneration was verified in 5-mm rat calvarial defects 8 weeks post-operation. Overall, this work developed an effective exosome delivery platform with improved exosome therapeutic functions, hence facilitating the clinical translation of exosome-based tissue engineering.

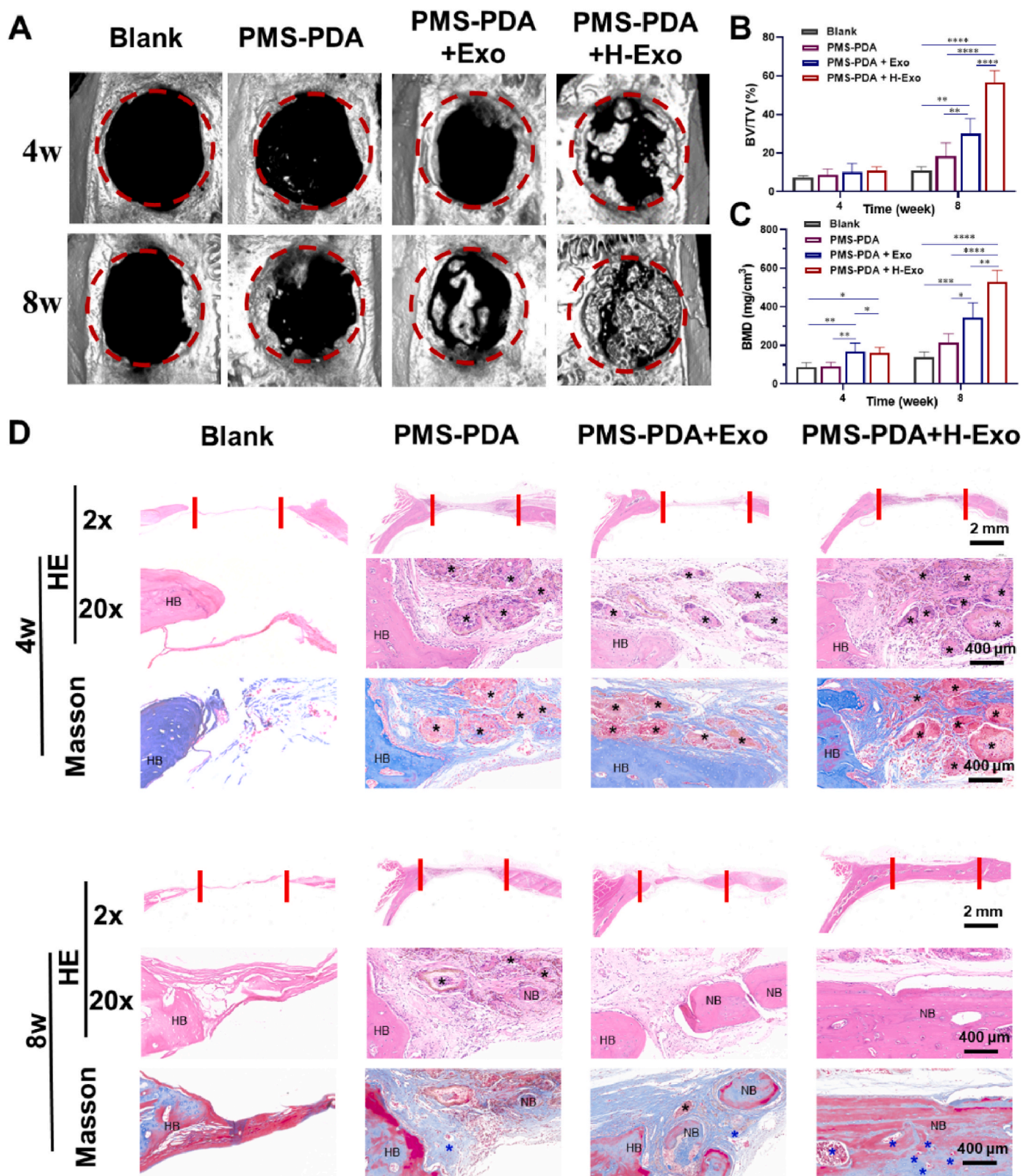
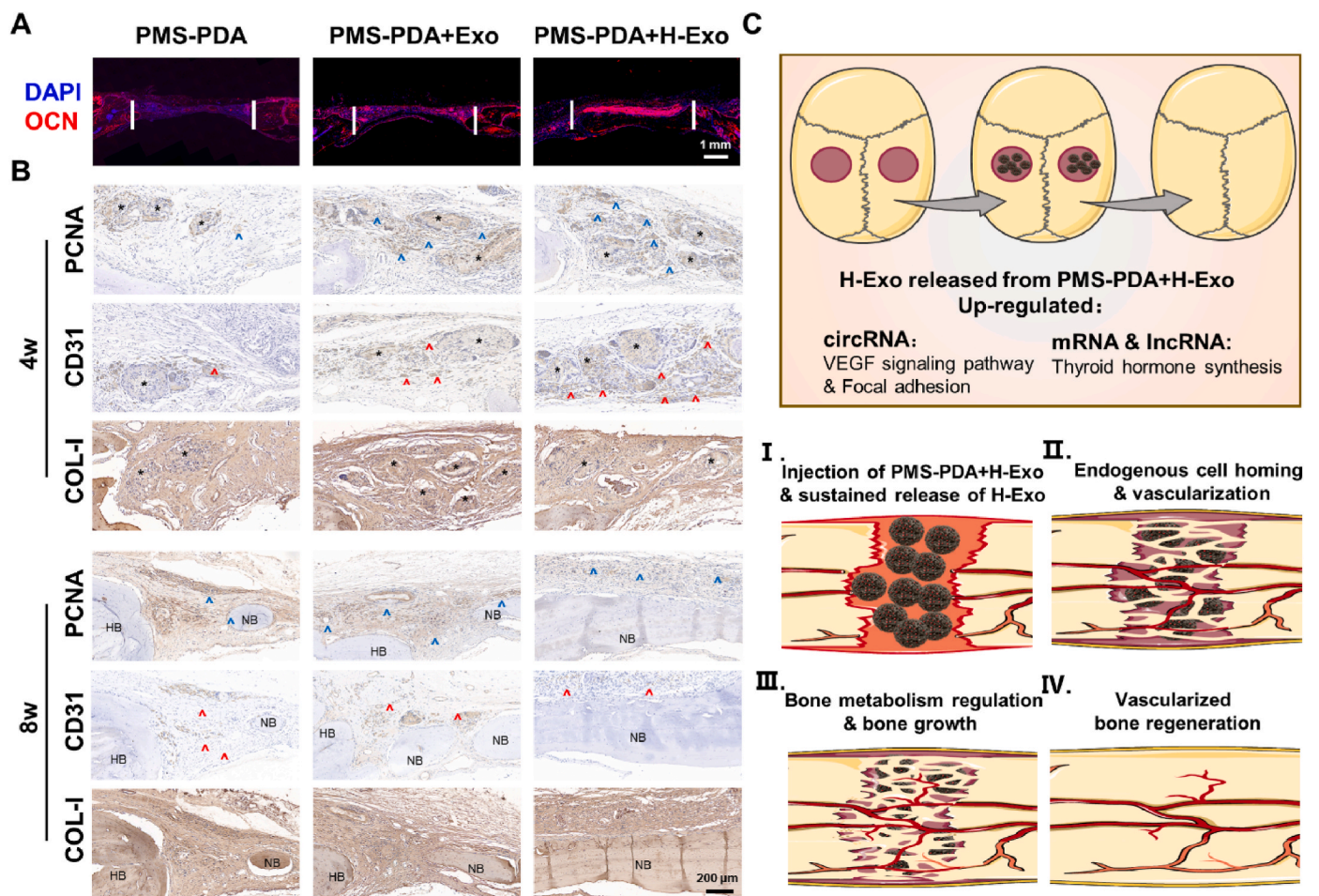


Fig. 4. PMS-PDA + H-Exo promotes calvarial bone regeneration. (A) Micro-CT images, (B) BV/TV values, and (C) BMD values of various microspheres filled defects. The diameter of red circles = 5 mm. (D) H&E and Masson's trichrome staining of calvarial bone sections filled with various microspheres. Black \* represents the location of residual microspheres, blue \* indicates the newly formed blood vessel, HB indicates the host bone (HB) and NB indicates the newly formed bone (NB).



**Fig. 5.** Histology evaluations on bone regeneration at 4 and 8 weeks post-operation for the groups filled with PMS-PDA, PMS-PDA + Exo or PMS-PDA + H-Exo. (A) OCN immunofluorescence staining, and (B) immunohistochemical including PCNA staining, CD31 staining and COL-I staining. Black \* represents the location of residual microspheres, Blue ^ indicates the positive staining of PCNA, red ^ indicates the positive staining of CD31, HB indicates the host bone (HB) and NB indicates the newly formed bone (NB). (C) The stepwise vascularized bone regeneration strategy through delivering H-Exo by PMS-PDA.

#### 4. Materials and methods

##### 4.1. Materials

PLGA (lactide: glycolide = 75:25,  $M_w = 50,000$ ) was obtained from Shandong Pharmaceutical Sciences Pilot Plant (China). Dopamine were purchased from Sigma-Aldrich (USA). Tris-HCl, surfactant (Span 80 and Tween 60), ammonium bicarbonate ( $\text{NH}_4\text{HCO}_3$ , analytical grade) and polyvinyl alcohol (PVA,  $M_w = 80,000$ ) were all purchased from Aladdin (China). All other chemical reagents and solvents were of analytical grade and supplied by Beijing Chemical Reagent Co., Ltd. (China)

##### 4.2. Cell culture

Normal exfoliated human deciduous incisors were collected from 6–7-year-old children under approved guidelines set by the National Institutes of Health Office of Human Subjects Research (PKUSSIRB-202057127). Cells in normoxia group were incubated at 37 °C in a humidified atmosphere containing 5%  $\text{CO}_2$  and 21%  $\text{O}_2$ , while hypoxia group cells were incubated at 37 °C, 5% humidity, 5%  $\text{CO}_2$  and 1%  $\text{O}_2$ . The culture medium was refreshed every 2 days. The detailed procedures for the isolation of SHEDs and culture of BMSCs and HUVECs are provided in Supplementary Information.

##### 4.3. Comprehensive proteomics analysis of Nor-SHEDs and Hypo-SHEDs

Cells ( $2 \times 10^6$ ) from each group (normoxia or hypoxia) were collected and kept at  $-80$  °C before being transferred to company for the whole protein quantitative proteomics analysis. The detailed procedures for the sample preparation and label-free data analysis are provided in Supplementary Information.

##### 4.4. Purification and identification of SHED-derived exosomes

SHEDs at passage 3 were utilized for exosome production. Exosomes were purified by several ultracentrifugation and filtration steps according to previous work [57], and the detailed procedures are shown in Supplementary Information. Two kinds of exosomes were gained from different culture conditions, named as Exo and H-Exo.

The relative concentration of suspended exosomes was detected by BCA protein Assay Kit (BCA; Thermo Fisher Scientific, America). The morphology of the extracted exosomes was inspected by a transmission electron microscope (TEM; Leica JEM-1400, America). Nanoparticle tracking analysis (NTA; Particle Metrix ZetaVIEW S/N 17–310, Germany) was used to determine the particle size. Western blot was performed to examine the specific exosomes markers CD9, HSP70 and TSG101 as well as cell lysates marker Calnexin.

#### 4.5. High-throughput sequence of Exo and H-Exo

Exosomes (200 ng) from each group (Exo or H-Exo) were collected and kept at  $-80^{\circ}\text{C}$  before subsequent ce-biochip based high-throughput sequence analyses. The detailed procedures for the RNA extraction, RNA amplification and labeling, gene expression hybridization, and data acquisition and analysis are provided in Supplementary Information.

#### 4.6. Preparation and characterizations of porous PDA modified PLGA microspheres

Porous PLGA microspheres were prepared according to previous works [58]. Briefly, 5 mL 0.05% w/v  $\text{NH}_4\text{HCO}_3$  aqueous solution and 20 mg Span 80 were added into 20 mL 5% w/v PLGA methylene chloride solution under ultrasonication for 3 min to form  $W_1/O$  primary emulsion. Subsequently, the  $W_1/O$  emulsion was dropped into 200 mL 1% w/v PVA solution containing 0.1% Tween 60 under continuous stirring (300 rpm) to generate  $W_1/O/W_2$  double emulsion. Four hours later, the solidified PLGA microspheres were washed with deionized water for three times, and immersed in 40 mL 0.1 M NaOH solution for 10 min, followed by washing with deionized water for five times and lyophilized to obtain the porous PLGA microspheres (termed as PMS).

To perform the surface modification with PDA, 1 g PMS were resuspended into a 50 mL dopamine solution (2 mg/mL in 10 mM Tris-HCl, pH 8.5) under continuous stirring (100 rpm) for 24 h. After the oxidative polymerization of dopamine, these microspheres turned into dark brown color, termed as PMS-PDA. Finally, PMS-PDA were washed with deionized water for five times and lyophilized for further characterizations and exosomes adsorption.

After sputtering with gold using a sputter-coater (Polaron E5600, USA), the morphology of PMS and PMS-PDA was observed by scanning electron microscope (SEM, JEOL JSM-7500F, Japan) at an accelerating voltage of 15 kV. In the meantime, the elemental mapping of oxygen (red) and nitrogen (green) was performed (exposure time: 180 s).

#### 4.7. Exosomes label and uptake by BMSCs and HUVECs

According to the manufacturer protocol, 5  $\mu\text{L}$  PKH26 and 1 mL Diluent C were added into exosomes at room temperature. After 5 min incubation, 1 mL FBS was applied to terminate the staining. Mixture was transferred to new ultracentrifuge tubes and ultracentrifuged (120,000g, 70 min) in dark place. The PKH26-positive exosomes were resuspended as mentioned before.

Afterwards, BMSCs or HUVECs were incubated with PKH26-positive exosomes in confocal dishes for 12 h. Then, cells were fixed in 4% paraformaldehyde for 15 min and stained nuclei using DAPI at room temperature. The internalization of exosomes by BMSCs or HUVECs were visualized by confocal microscopy (TCS-SP8 STED 3X; Leica, America).

#### 4.8. Exosomes adsorption and release assay

Prior to exosomes adsorption, microspheres were sterilized by being exposed to ultraviolet light for 12 h, and the morphology will not be deformed. In addition, the exosomes adsorption procedure was also performed under aseptic conditions.

To compare the ability of exosomes adsorption between PMS and PMS-PDA, 10 mL H-Exo (1000  $\mu\text{g}/\text{mL}$ ) were added to 200 mg PMS or PMS-PDA in 15 mL tubes and incubated at  $4^{\circ}\text{C}$  for 1–6 h. To visualize the distribution of exosomes in microspheres, the PKH26 positive exosomes were adsorbed by PMS-PDA according to the same procedure. The adsorption kinetic of exosomes was examined at predetermined time-points (1, 2, 3, 4, 5, and 6 h post-adsorption) after microspheres were washed with PBS for three times. At specific time points, 100  $\mu\text{L}$  supernatant was collected and concentration of suspended exosomes were detected by BCA protein Assay Kit.

To accumulate the release curve of PMS and PMS-PDA, after reaching the maximum adsorption rate (6 h for PMS, and 4 h for PMS-PDA) and washed with PBS for three times, 2 mg microsphere-exosome complexes were soaked in 100  $\mu\text{L}$  PBS and incubated at a horizontal shaker at  $37 \pm 1^{\circ}\text{C}$ , 60 rpm for 21 days. At predetermined timepoints (day 1, 3, 5, 7, 14 and 21), 80  $\mu\text{L}$  supernatant was collected and the system was replenished with 80  $\mu\text{L}$  fresh PBS, the concentration of exosomes in the supernatant was detected by BCA protein assay Kit.

#### 4.9. Cell viability

BMSCs were seeded onto 96-well plates with a density of 1000 cells/well in the presence of exosomes (Exo or H-Exo, 10  $\mu\text{g}/\text{mL}$ ) or various microspheres (PMS, PMS-PDA, PMS-PDA + Exo, or PMS-PDA + H-Exo, 2 mg/well) for 1, 3 and 5 days to evaluate cell proliferation with Cell Counting Kit-8 (CCK-8; Dojindo, Japan). Cells were washed with PBS and replaced by 10% (v/v) CCK-8 solution for a 1 h-dark-treatment to measure optical density (OD) values. For live/dead staining assay, at day 5, a live-dead staining kit (Beyotime, China) was performed to evaluate the cytotoxicity of various microspheres according to the manufacturer's instruction.

#### 4.10. Cell migration

To evaluate cell migration, wound healing assay and Transwell assay were conducted. For wound healing assay, BMSCs or HUVECs were seeded in 24-well plates at a density of 5000 cells/well. Twenty-four hours after cells being seeded, a series of 1.5 mm-linear wound were scratched by blue tip and washed with PBS for three times. Culture medium containing 10  $\mu\text{g}/\text{mL}$  exosomes (Exo or H-Exo) and 1% FBS were added to continue the incubation for another 24 h. Wound closer was observed by an optical microscope and analyzed using ImageJ software. For transwell assay,  $1 \times 10^5$  BMSCs or HUVECs were seeded onto the upper chamber with 8- $\mu\text{m}$  pore filters (Corning). Conditional medium (500  $\mu\text{L}$ ) containing 10  $\mu\text{g}/\text{mL}$  exosomes (Exo or H-Exo) was added. After incubated for 24 h, cells were fixed with 4% paraformaldehyde and unmigrated cells were gently wiped using a cotton tip. Then, 1% crystal violet was used to stain the migrated cells for 30 min. The relative numbers of migrated cells were counted and analyzed in five randomly microscopic fields per filter.

#### 4.11. In vitro osteogenic differentiation

BMSCs were seeded in 24-well plates at a density of 5000 cells/well, and the culture medium was replaced by osteogenic induction culture medium (OM:  $\alpha$ -MEM, 10% FBS, 10 nM dexamethasone, 20 mM  $\beta$ -glycerophosphate and 100  $\mu\text{M}$  ascorbic acid) when the confluence reached 80% [59]. Wells were randomly divided into three groups: 1) OM as control group; 2) OM supplemented with 10  $\mu\text{g}/\text{mL}$  Exo; 3) OM supplemented with 10  $\mu\text{g}/\text{mL}$  H-Exo. Cells were washed with PBS and fixed in 4% paraformaldehyde for 15 min at room temperature at each time point (day 7 and 14) for further analysis. For ALP staining, the cells were stained with BCIP/NBT Kit (C3206; Solarbio, China) for 15 min and washed with distilled water. Protein of ALP was tested by ALP Assay Kit (P0321S; Solarbio, China). For alizarin red staining, the cells were stained with a solution of alizarin red working solution (1%, w/v, G1452; Solarbio, China) for 10 min and washed with distilled water. The calcium content was detected by Calcium Colorimetric Assay Kit (S1063S; Beyotime, China) after extracting the protein by RIPA. The detailed procedures for the ALP and alizarin red staining of BMSCs induced by various microspheres are shown in Supplementary Information.

For the quantitative real time polymerase chain reaction (qRT-PCR) assay, Trizol (ThermoFisher, America) and Prime Script RT reagent Kit (RR036A; Takara, Japan) were carefully used to extract RNA and reverse it to cDNA (complementary DNA) after 7 days of osteoinductive culture.

Diluted cDNA was mixed with PowerUp™ SYBR™ GREEN Master Mix (A25742; ThermoFisher, America), RNase free water (DEPC water) and primers to perform qRT-PCR (ABI7500; ThermoFisher, America). Three gene markers (bonemorphogenic protein-2 (BMP-2), runt-related transcription factor 2 (RUNX2), and osteocalcin (OCN)) were evaluated, and GAPDH were used as an internal control, their specific primers were listed in Table S3.

#### 4.12. *In vitro* and *In vivo* angiogenesis assay

For tube formation assay, HUVECs ( $2 \times 10^4$  cells/mL) were suspended in the condition medium supplemented with exosomes (Exo or H-Exo, 10  $\mu$ g/mL), and then seeded in 96-well plate precoated with Matrigel (70  $\mu$ L/well). Images were captured after 6 h and the newly formed endothelial tubes were analyzed by ImageJ. The VEGF and VEGF-R2 gene expression of HUVECs were test via qRT-PCR after 3 days culture with the same procedure mentioned above.

For chick embryo chorioallantoic membrane (CAM) assay, Chicken eggs were received at day 0 and incubated for five days at 38.3 °C with constant humidity. On day 5, eggs were rinsed with 70% ethanol, and egg shells were prized up to open a  $1.5 \times 1.5$  cm<sup>2</sup> surgical field. Then, embryo chorioallantoic membrane was torn off under aseptic conditions, and 100  $\mu$ L exosomes (Exo or H-Exo, 10  $\mu$ g/mL) or 20 mg microspheres (PMS, PMS-PDA, PMS-PDA + Exo, or PMS-PDA + H-Exo) were applied to each egg. PBS treatment was set as control. After 5 days incubation, the embryos were fixed and observed by an inverted fluorescence microscope, the newly formed vessels were analyzed by ImageJ.

#### 4.13. *In vivo* bone regeneration using a rat calvarial defect model

Animal experiments were sanctioned by the Peking University Animal Care and Use Committee (LA2020483) and operations were in accordance with the institutional animal guidelines. 5 mm-calvarial defects were operated on 6-week-old male SD rats which were accommodated in a specific pathogen-free (SPF) environment. The total 32 rats were randomly separated into five groups: 1) control group with normal saline treatment (control, n = 8); 2) PDA coating porous PLGA microsphere (PMS-PDA, n = 8); 3) and normal exosomes loaded PMS-PDA treatment (PMS-PDA + Exo, n = 8); 4) hypoxia exosomes loaded PMS-PDA treatment (PMS-PDA + H-Exo, n = 8). At predetermined time-points (4 and 8 weeks), rats were sacrificed by CO<sub>2</sub> inhalation. The calvaria were harvested and fixed with 4% paraformaldehyde for 72 h. Micro-CT scanner (Siemens, Germany) was used to assess the new bone formation by indicators such as bone mineral density (BMD) and the ratio of new bone volume to tissue volume (BV/TV). Hematoxylin & eosin (HE) and Masson staining were performed to evaluate the new bone formation, and the sections were observed from coronal plane. Immunofluorescence analysis of osteogenesis-associated protein OCN and immunohistochemical staining of PCNA, CD31 and COL-I were evaluated to further reveal the new bone formation. The detailed procedures for animal experiments are provided in Supplementary Information.

#### 4.14. Statistical analysis

All quantitative data were expressed as mean  $\pm$  standard deviation (SD) for n  $\geq$  3. Statistical analysis was carried out using one-way/two-way analysis of variance (ANOVA) with Tukey's test. Differences between groups of \*p < 0.05 were considered statistically significant, \*\*p < 0.01 and \*\*\*p < 0.001 were considered highly significant.

#### CRediT authorship contribution statement

**Yike Gao:** Conceptualization, Investigation, Methodology, Formal analysis, Writing – original draft. **Zuoying Yuan:** Conceptualization,

Investigation, Methodology, Writing – original draft. **Xiaoqing Yuan:** Formal analysis. **Zhuo Wan:** Investigation. **Yingjie Yu:** Writing – review & editing. **Qi Zhan:** Formal analysis. **Yuming Zhao:** Supervision, Data curation, Funding acquisition. **Jianmin Han:** Resources. **Jianyong Huang:** Resources, Funding acquisition. **Chunyang Xiong:** Project administration. **Qing Cai:** Supervision, Writing – review & editing.

#### Declaration of competing interest

The authors declare that there is no conflict of interest in this manuscript.

#### Acknowledgements

The authors acknowledged the financial support from Beijing Natural Science Foundation (7212135), and National Natural Science Foundation of China (NSFC) (11972001, 11972002 and 12072001). We thank Dr. Jianlin Chen from College of Engineering, Peking University, for the Micro-CT analysis.

#### Appendix B. Supplementary data

Supplementary data to this article can be found online at <https://doi.org/10.1016/j.bioactmat.2022.01.041>.

#### References

- [1] C.M. Madl, S.C. Heilshorn, H.M. Blau, Bioengineering strategies to accelerate stem cell therapeutics, *Nature* 557 (2018) 335–342.
- [2] I. Martin, J. Galipeau, C. Kessler, K. Le Blanc, F. Dazzi, Challenges for mesenchymal stromal cell therapies, *Sci. Transl. Med.* 11 (2019), eaat2189.
- [3] M.E. Wechsler, V.V. Rao, A.N. Borelli, K.S. Anseth, Engineering the MSC secretome: a hydrogel focused approach, *Adv. Healthc. Mater.* 10 (2021) 2001948.
- [4] X.X. Li, X.J. Yuan, Y. Zhai, S. Yu, R.X. Jia, L.P. Yang, Z.Z. Ma, Y.M. Zhao, Y. X. Wang, L.H. Ge, Treatment with stem cells from human exfoliated deciduous teeth and their derived conditioned medium improves retinal visual function and delays the degeneration of photoreceptors, *Stem Cell. Dev.* 28 (2019) 1514–1526.
- [5] R. Kalluri, V.S. LeBleu, The biology, function, and biomedical applications of exosomes, *Science* 367 (2020), eaau6977.
- [6] T. Yamamoto, N. Kosaka, T. Ochiya, Latest advances in extracellular vesicles: from bench to bedside, *Sci. Technol. Adv. Mater.* 20 (2019) 746–757.
- [7] A.K.A. Silva, S. Perretta, G. Perrod, L. Pidial, V. Lindner, F. Carn, S. Lemieux, D. Alloeyau, I. Boucenna, P. Menasche, B. Dallemagne, F. Gazeau, C. Wilhelm, C. Cellier, O. Clement, G. Rahmi, Thermoresponsive gel embedded with adipose stem-cell-derived extracellular vesicles promotes esophageal fistula healing in a thermo-actuated delivery strategy, *ACS Nano* 12 (2018) 9800–9814.
- [8] O.P.B. Wiklander, M.A. Brennan, J. Lotvall, X.O. Breakefield, S. EL Andaloussi, Advances in therapeutic applications of extracellular vesicles, *Sci. Transl. Med.* 11 (2019) eaav8521.
- [9] A. Nagelkerke, M. Ojansivu, L. van der Koog, T.E. Whittaker, E.M. Cunnane, A. M. Silva, N. Dekker, M.M. Stevens, Extracellular vesicles for tissue repair and regeneration: evidence, challenges and opportunities, *Adv. Drug Deliv. Rev.* 175 (2021) 113775.
- [10] P.A. Shiekh, A. Singh, A. Kumar, Exosome laden oxygen releasing antioxidant and antibacterial cryogel wound dressing OxOBand alleviate diabetic and infectious wound healing, *Biomaterials* 249 (2020) 120020.
- [11] H.P. Bei, P.M. Hung, H.L. Yeung, S. Wang, X. Zhao, Bone-a-Petite: engineering exosomes towards bone, osteochondral, and cartilage repair, *Small* (2021), e2101741, <https://doi.org/10.1002/smll.202101741>.
- [12] X. Xing, S. Han, Z. Li, Z. Li, Emerging role of exosomes in craniofacial and dental applications, *Theranostics* 10 (2020) 8648–8664.
- [13] J.B. Fan, C.S. Lee, S. Kim, C. Chen, T. Aghaloo, M. Lee, Generation of small RNA-modulated exosome mimetics for bone regeneration, *ACS Nano* 14 (2020) 11973–11984.
- [14] D. Lopes, C. Martins-Cruz, M.B. Oliveira, J.F. Mano, Bone physiology as inspiration for tissue regenerative therapies, *Biomaterials* 185 (2018) 240–275.
- [15] M.A. Brennan, P. Layrolle, D.J. Mooney, Biomaterials functionalized with MSC secreted extracellular vesicles and soluble factors for tissue regeneration, *Adv. Funct. Mater.* 30 (2020) 1909125.
- [16] L. Fu, L. Zhang, X. Zhang, L. Chen, Q. Cai, X. Yang, Roles of oxygen level and hypoxia-inducible factor signaling pathway in cartilage, bone and osteochondral tissue engineering, *Biomed. Mater.* 16 (2021), 022006.
- [17] J.R.K. Samal, V.K. Rangasami, S. Samanta, O.P. Varghese, O.P. Oommen, Discrepancies on the role of oxygen gradient and culture condition on mesenchymal stem cell fate, *Adv. Healthc. Mater.* 10 (2021) 2002058.
- [18] Y. Rong, J. Zhang, D. Jiang, C. Ji, W. Liu, J. Wang, X. Ge, P. Tang, S. Yu, W. Cui, W. Cai, Hypoxic pretreatment of small extracellular vesicles mediates cartilage

- repair in osteoarthritis by delivering miR-216a-5p, *Acta Biomater.* 122 (2021) 325–342.
- [19] W. Liu, L. Li, Y. Rong, D. Qian, J. Chen, Z. Zhou, Y. Luo, D. Jiang, L. Cheng, S. Zhao, F. Kong, J. Wang, Z. Zhou, T. Xu, F. Gong, Y. Huang, C. Gu, X. Zhao, J. Bai, F. Wang, W. Zhao, L. Zhang, X. Li, G. Yin, J. Fan, W. Cai, Hypoxic mesenchymal stem cell-derived exosomes promote bone fracture healing by the transfer of miR-126, *Acta Biomater.* 103 (2020) 196–212.
- [20] C. Liu, C. Su, Design strategies and application progress of therapeutic exosomes, *Theranostics* 9 (2019) 1015–1028.
- [21] V.P. Murali, C.A. Holmes, Biomaterial-based extracellular vesicle delivery for therapeutic applications, *Acta Biomater.* 124 (2021) 88–107.
- [22] L. Li, Y. Zhang, J. Mu, J. Chen, C. Zhang, H. Cao, J. Gao, Transplantation of human mesenchymal stem-cell-derived exosomes immobilized in an adhesive hydrogel for effective treatment of spinal cord injury, *Nano Lett.* 20 (2020) 4298–4305.
- [23] E.A. Mol, Z. Lei, M.T. Roefs, M.H. Bakker, M.J. Goumans, P.A. Doevendans, P.Y. W. Dankers, P. Vader, J.P.G. Sluijter, Injectable supramolecular ureidopyrimidinone hydrogels provide sustained release of extracellular vesicle therapeutics, *Adv. Healthc. Mater.* 8 (2019), e1900847.
- [24] C. Wang, M. Wang, K. Xia, J. Wang, F. Cheng, K. Shi, L. Ying, C. Yu, H. Xu, S. Xiao, C. Liang, F. Li, B. Lei, Q. Chen, A bioactive injectable self-healing anti-inflammatory hydrogel with ultralong extracellular vesicles release synergistically enhances motor functional recovery of spinal cord injury, *Bioact. Mater.* 6 (2021) 2523–2534.
- [25] W.B. Swanson, T. Gong, Z. Zhang, M. Eberle, D. Niemann, R. Dong, K.J. Ramhbia, P.X. Ma, Controlled release of odontogenic exosomes from a biodegradable vehicle mediates dentinogenesis as a novel biomimetic pulp capping therapy, *J. Contr. Release* 324 (2020) 679–694.
- [26] Z. Hu, C. Ma, X. Rong, S. Zou, X. Liu, Immunomodulatory ECM-like microspheres for accelerated bone regeneration in diabetes mellitus, *ACS Appl. Mater. Interfaces* 10 (2018) 2377–2390.
- [27] T. Fang, Z. Yuan, Y. Zhao, X. Li, Y. Zhai, J. Li, X. Wang, N. Rao, L. Ge, Q. Cai, Synergistic effect of stem cells from human exfoliated deciduous teeth and rhBMP-2 delivered by injectable nanofibrous microspheres with different surface modifications on vascularized bone regeneration, *Chem. Eng. J.* 370 (2019) 573–586.
- [28] C.-S. Lee, S. Kim, J. Fan, H.S. Hwang, T. Aghaloo, M. Lee, Smoothed agonist sterosome immobilized hybrid scaffold for bone regeneration, *Sci. Adv.* 6 (2020) eaaz7822.
- [29] W. Li, Y. Liu, P. Zhang, Y. Tang, M. Zhou, W. Jiang, X. Zhang, G. Wu, Y. Zhou, Tissue-engineered bone immobilized with human adipose stem cells-derived exosomes promotes bone regeneration, *ACS Appl. Mater. Interfaces* 10 (2018) 5240–5254.
- [30] Z. Yuan, P. Wei, Y. Huang, W. Zhang, F. Chen, X. Zhang, J. Mao, D. Chen, Q. Cai, X. Yang, Injectable PLGA microspheres with tunable magnesium ion release for promoting bone regeneration, *Acta Biomater.* 85 (2019) 294–309.
- [31] Z. Yuan, X. Yuan, Y. Zhao, Q. Cai, Y. Wang, R. Luo, S. Yu, Y. Wang, J. Han, L. Ge, J. Huang, C. Xiong, Injectable GelMA cryogel microspheres for modularized cell delivery and potential vascularized bone regeneration, *Small* 17 (2021), e2006596.
- [32] A.C. Daly, L. Riley, T. Segura, J.A. Burdick, Hydrogel microparticles for biomedical applications, *Nat. Rev. Mater.* 5 (2019) 20–43.
- [33] P. Wei, W. Jing, Z. Yuan, Y. Huang, B. Guan, W. Zhang, X. Zhang, J. Mao, Q. Cai, D. Chen, X. Yang, Vancomycin- and strontium-loaded microspheres with multifunctional activities against bacteria, in angiogenesis, and in osteogenesis for enhancing infected bone regeneration, *ACS Appl. Mater. Interfaces* 11 (2019) 30596–30609.
- [34] N. Haque, N.H.A. Kasim, Stem cells from human exfoliated deciduous teeth: waste to wealth, *Curr. Stem Cell Res. Ther.* 16 (2021) 493–494.
- [35] S. Yildirim, N. Zibandeh, D. Genc, E.M. Ozcan, K. Goker, T. Akkoc, The Comparison of the immunologic properties of stem cells isolated from human exfoliated deciduous teeth, dental pulp, and dental follicles, *Stem Cell. Int.* (2016) 4682875, 2016.
- [36] M. Miura, S. Gronthos, M. Zhao, B. Lu, L.W. Fisher, P.G. Robey, S. Shi, SHED: stem cells from human exfoliated deciduous teeth, *Proc. Natl. Acad. Sci. U.S.A.* 100 (2003) 5807–5812.
- [37] R. Kunimatsu, K. Nakajima, T. Awada, Y. Tsuka, T. Abe, K. Ando, T. Hiraki, A. Kimura, K. Tanimoto, Comparative characterization of stem cells from human exfoliated deciduous teeth, dental pulp, and bone marrow-derived mesenchymal stem cells, *Biochem. Biophys. Res. Commun.* 501 (2018) 193–198.
- [38] Y. Li, J.K. Xu, J. Mi, X. He, Q. Pan, L.Z. Zheng, H.Y. Zu, Z.Y. Chen, B.Y. Dai, X. Li, Q. Q. Pang, L. Zou, L.B. Zhou, L. Huang, W.X. Tong, G. Li, L. Qin, Biodegradable magnesium combined with distraction osteogenesis synergistically stimulates bone tissue regeneration via CGRP-FAK-VEGF signaling axis, *Biomaterials* 275 (2021).
- [39] Y.T. Wang, Y.J. Yang, X.L. Wang, T. Yoshitomi, N. Kawazoe, Y.N. Yang, G.P. Chen, Micropattern-controlled chirality of focal adhesions regulates the cytoskeletal arrangement and gene transfection of mesenchymal stem cells, *Biomaterials* 271 (2021) 120984.
- [40] H.Y. Kim, S. Mohan, Role and mechanisms of actions of thyroid hormone on the skeletal development, *Bone Res* 1 (2013) 146–161.
- [41] V.D. Leitch, J.H.D. Bassett, G.R. Williams, Role of thyroid hormones in craniofacial development, *Nat. Rev. Endocrinol.* 16 (2020) 147–164.
- [42] J. Wu, L. Chen, R. Wang, Z. Song, Z. Shen, Y. Zhao, S. Huang, Z. Lin, Exosomes secreted by stem cells from human exfoliated deciduous teeth promote alveolar bone defect repair through the regulation of angiogenesis and osteogenesis, *ACS Biomater. Sci. Eng.* 5 (2019) 3561–3571.
- [43] A.K. Gaharwar, I. Singh, A. Khademhosseini, Engineered biomaterials for in situ tissue regeneration, *Nat. Rev. Mater.* 5 (2020) 686–705.
- [44] S.J. Wang, D. Jiang, Z.Z. Zhang, Y.R. Chen, Z.D. Yang, J.Y. Zhang, J. Shi, X. Wang, J.K. Yu, Biomimetic nanosilica-collagen scaffolds for in situ bone regeneration: toward a cell-free, one-step surgery, *Adv. Mater.* 31 (2019), e1904341.
- [45] Z. Lin, D. Shen, W. Zhou, Y. Zheng, T. Kong, X. Liu, S. Wu, P.K. Chu, Y. Zhao, J. Wu, K.M.C. Cheung, K.W.K. Yeung, Regulation of extracellular bioactive cations in bone tissue microenvironment induces favorable osteoimmune conditions to accelerate in situ bone regeneration, *Bioact. Mater.* 6 (2021) 2315–2330.
- [46] L. Fan, P. Guan, C. Xiao, H. Wen, Q. Wang, C. Liu, Y. Luo, L. Ma, G. Tan, P. Yu, L. Zhou, C. Ning, Exosome-functionalized polyetheretherketone-based implant with immunomodulatory property for enhancing osseointegration, *Bioact. Mater.* 6 (2021) 2754–2766.
- [47] S. Hu, Z. Li, D. Shen, D. Zhu, K. Huang, T. Su, P.-U. Dinh, J. Cores, K. Cheng, Exosome-eluting stents for vascular healing after ischaemic injury, *Nat. Biomed. Eng.* 5 (2021) 1174–1188.
- [48] F. Wei, M. Li, R. Crawford, Y. Zhou, Y. Xiao, Exosome-integrated titanium oxide nanotubes for targeted bone regeneration, *Acta Biomater.* 86 (2019) 480–492.
- [49] N. Su, Y. Hao, F. Wang, W. Hou, H. Chen, Y. Luo, Mesenchymal stromal exosome-functionalized scaffolds induce innate and adaptive immunomodulatory responses toward tissue repair, *Sci. Adv.* 7 (2021), eabf7207.
- [50] Z. Yuan, Z. Wan, P. Wei, X. Lu, J. Mao, Q. Cai, X. Zhang, X. Yang, Dual-controlled release of icariin/Mg(2+) from biodegradable microspheres and their synergistic upregulation effect on bone regeneration, *Adv. Healthc. Mater.* 9 (2020), e2000211.
- [51] Y. Deng, W.Z. Yang, D. Shi, M.J. Wu, X.L. Xiong, Z.G. Chen, S.C. Wei, Bioinspired and osteopromotive polydopamine nanoparticle-incorporated fibrous membranes for robust bone regeneration, *NPG Asia Mater.* 11 (2019) 39.
- [52] L. Cao, Y. Zhang, M.Y. Qian, X.P. Wang, Q.Z. Shuai, C. Gao, R. Lang, J. Yang, Construction of multicellular aggregate by E-cadherin coated microparticles enhancing the hepatic specific differentiation of mesenchymal stem cells, *Acta Biomater.* 95 (2019) 382–394.
- [53] M. Ge, Y.Q. Sheng, S.Y. Qi, L. Cao, Y. Zhang, J. Yang, PLGA/chitosan-heparin composite microparticles prepared with microfluidics for the construction of hMSC aggregates, *J. Mater. Chem. B* 8 (2020) 9921–9932.
- [54] Z.Y. Du, H.J. Leng, L.Y. Guo, Y.Q. Huang, T.Y. Zheng, Z.D. Zhao, X. Liu, X. Zhang, Q. Cai, X.P. Yang, Calcium silicate scaffolds promoting bone regeneration via the doping of Mg<sup>2+</sup> or Mn<sup>2+</sup> ion, *Composites, Part B* 190 (2020) 107937.
- [55] J. Liu, G. Chen, H. Xu, K. Hu, J. Sun, M. Liu, F. Zhang, N. Gu, Pre-vascularization in fibrin Gel/PLGA microsphere scaffolds designed for bone regeneration, *NPG Asia Mater.* 10 (2018) 827–839.
- [56] A. Liu, D. Lin, H. Zhao, L. Chen, B. Cai, K. Lin, S.G. Shen, Optimized BMSC-derived osteoinductive exosomes immobilized in hierarchical scaffold via lyophilization for bone repair through Bmpr2/Acvr2b competitive receptor-activated Smad pathway, *Biomaterials* 272 (2021) 120718.
- [57] Q. Zhan, K.K. Yi, X.P. Li, X.T. Cui, E.Y. Yang, N. Chen, X.B. Yuan, J. Zhao, X. Hou, C.S. Kang, Phosphatidylcholine-engineered exosomes for enhanced tumor cell uptake and intracellular antitumor drug delivery, *Macromol. Biosci.* 21 (2021) 2100042.
- [58] Y. Yuan, X. Shi, Z. Gan, F. Wang, Modification of porous PLGA microspheres by poly-l-lysine for use as tissue engineering scaffolds, *Colloids Surf., B* 161 (2018) 162–168.
- [59] X. Li, S. Li, H. Qi, D. Han, N. Chen, Q. Zhan, Z. Li, J. Zhao, X. Hou, X. Yuan, X. Yang, Early healing of alveolar bone promoted by microRNA-21-loaded nanoparticles combined with Bio-Oss particles, *Chem. Eng. J.* 401 (2020) 126026.